Geomechanics and Engineering, *Vol. 38, No. 3 (2024) 215-229*
https://doi.org/10.12989/gae.2024.38.3.215

Mine water inrush characteristics based on RQD index of rock mass and multiple types of water channels

Jinhai Zhao*[1,2], Weilong Zhu[1,2a], Wenbin Sun[1,2b], Changbao Jiang[1,2,3c], Hailong Ma[1,2d] and Hui Yang[1,2e]

[1]*State Key Laboratory Breeding Base for Mining Disaster Prevention and Control, Shandong University of Science and Technology, Qingdao 266590, China*
[2]*College of Energy and Mining Engineering, Shandong University of Science and Technology, Qingdao 266590, China*
[3]*State Key Laboratory of Coal Mine Disaster Dynamics and Control, School of Resources and Safety Engineering, Chongqing University, Chongqing 400030, China*

(*Received July 21, 2023, Revised July 10, 2024, Accepted July 15, 2024*)

Abstract. Because of the various patterns of deep-water inrush and complicated mechanisms, accurately predicting mine water inflows is always a difficult problem for coal mine geologists. In study presented in this paper, the water inrush channels were divided into four basic water diversion structures: aquifer, rock fracture zone, fracture zone and goaf. The fluid flow characteristics in each water-conducting structure were investigated by laboratory tests, and multistructure and multisystem coupling flow analysis models of different water-conducting structures were established to describe the entire water inrush process. Based on the research of the water inrush flow paths, the analysis model of different water inrush space structures was established and applied to the prediction of mine water inrush inflow. The results prove that the conduction sequence of different water-conducting structures and the changing rule of permeability caused by stress changes before and after the peak have important influences on the characteristics of mine water-gushing. Influenced by the differences in geological structure and combined with rock mass RQD and fault conductivity characteristics and other mine exploration data, the prediction of mine water inflow can be realized accurately. Taking the water transmitting path in the multistructure as the research object of water inrush, breaking through the limitation of traditional stratigraphic structure division, the prediction of water inflow and the estimation of potentially flooded area was realized, and water bursting intensity was predicted. It is of great significance in making reasonable emergency plans.

Keywords: broken rock mass; rough surface cracks; stress and strain; water conduction structure; water inflow prediction

1. Introduction

Mine inflow, a key component of for mining design and mine water treatment, refers to the total amount of water flowing into the tunnel from surface water, crevice water, goaf water and karst errors between the predicted water inflow made during the prospecting stage and the actual water inflow after mining can exceed 50%, and some errors even reach dozens of times (Zhang 2009, Adhikary 2012).

Accurate forecasting of mine inflow remains a thorny puzzle for coal mine geologists. Numerical methods have been used to address complex mining situations (Li *et al.* 2011, Mengistu *et al.* 2015, Singh and Woolhiser 2002, Voss 2011, Komurlu *et al.* 2016, Lawal *et al.* 2022, Mahmoodzadeh *et al.* 2022, Ma *et al.* 2023), and graphical tools that facilitate the construction of complex models have been developed as computers have become more powerful and groundwater flow codes have become more standardized (Bredehoeft 2005, Kazemi 2012, Vandenbohede *et al.* 2011, Ghyasvand *et al.* 2022, Vaziri *et al.* 2022). In addition, mine water inrush will also lead to water shortages and groundwater pollution, which will cause great risks to the safe use of water resources (Huang *et al.* 2019, Ma *et al.* 2017, Liu *et al.* 2017).

However, it is still very difficult to reasonably and accurately forecast the change in water inflow and pollution during mine construction and production (Bouzourra *et al.* 2015, Chen *et al.* 2021, Gu *et al.* 2020).

Most of the existing theories are qualitative analyses on water inrush prevention from the perspective of the safety factor, such as the effective aquifuge theory and water bursting coefficient method (Shi 2009, Hasiniaina *et al.* 2010, Battumur 2009). Other theories offer explanations and explorations based on the integrity of the bottom plate space structure. For example, theories on three underlying belts and four underlying belts subtract the destroyed rock

*Corresponding author, Professor
E-mail: Jinhai.zhao@sdust.edu.cn
[a]Master
E-mail: zwl0315224@163.com
[b]Professor
E-mail: swb@sdust.edu.cn
[c]Professor
E-mail: jcb@cqu.edu.cn
[d]Master
E-mail: 1766124758@qq.com
[e]Ph.D.
E-mail: 837784880@qq.com

ISSN: 2005-307X (Print), 2092-6219 (Online)

stratum based on the existing aquiclude effect and thus finally determine a relative safety factor. These theories are still qualitative forecasts. The aforementioned methods can determine the statistical probability significance of water inrush. However, it is difficult for them to accurately identify the location of water inrush, let alone to forecast water inflow (Bouzourra *et al.* 2015, Chen *et al*. 2021).

Mine inflow is featured by the flow mechanism of mine water in the water diversion channel. Only by understanding the flow rules and influencing factors of mine water in various water diversion channels can geologists carry out quantitative calculations of water inflow and potential flooded areas. In regard to mine inflow forecasting, the mine water content coefficient analogy method, the hydrodynamic method in narrow horizontal channels, and the large well method to determine the roof water inflow were adopted (Hasiniaina *et al.* 2010, Wu 2014). The water inflow determined by using Dupuit's equation and detection of the water-rich zone in the roof of the first mining working face by transient electromagnetic mining exploration was calculated, and the mine inflow was predicted by the fracture development law (Hou *et al*. 2016). The numerical simulation of roof water inflow by Visual Modflow and the calculation of mine inflow under natural mining conditions were conducted (Blum *et al.* 2009). Methods to forecast mine inflow can be mainly divided into two categories according to comprehensive analysis. One category encompasses deterministic mathematical model methods, mainly including the water balance method, the analytical method and the numerical method. The other category encompasses statistical analysis methods, mainly including the hydrogeological analogue method, the correlational analysis method and the time series analysis method (Hasiniaina *et al.* 2010, Wu 2014, Battumur 2009, Ibishi *et al*. 2022, Khorasani *et al*. 2019).

The current major problems in mine inflow forecasting and calculation are as follows. ① Mine inflow is characterized by nonlinearity. The current quantitative forecasting method is based on Darcy's law. However, it cannot be applied to the realistic characteristics of mine inflow. ② Research on the dynamic variation rule of water inflow during mining should be deepened. The variations in geological and hydrogeological conditions will cause changes in mechanical equilibrium in underground rock masses that will exert a direct influence upon the amount and change process of water inflow. Therefore, research on the influence of the mining process on seepage characteristics in the water diversion channel serves as the key to precisely forecasting mine inflow

With the development of geophysical exploration technology, it is possible to solve the two major problems (geological structure prospecting (concerning water source and carrier characteristics) and water flow motion law) that restrict mine inflow forecasting through using fine exploration and comprehensive knowledge of underground conditions. The most important tasks for coal miners are to research the water diversion characteristics and dynamic variation rule of water diversion channels during the process of mining and then reveal both the mechanism and process of sudden mine inflow. In view of the relationship between the RQD rock mass categorization method and permeability, the permeability difference before and after the rock mass stress peak has been considered based on fine fault exploration data to reveal the influence of fluid-structure interaction, master the law of confined water transport and movement at different mining time points and in various types of water diversion channels, and forecast mine inflow. Thus, mine inflow can be monitored to realize the quantitative forecasting of mine inflow and water inrush, which is of great significance in making reasonable water inrush emergency management plans

2. Categorization of floor water diversion channel

In terms of the division of basic mine water diversion structures, there are four types of dominant water inrush surfaces: strong runoff zones of floor limestone, water conduction zones, mining-induced faults and floor fracture zones (Gao *et al.* 2009). The floor water inrush mode can be divided into three types, namely, crack extension, fracture structure extension and conduction, and the primary channel (Guo *et al.* 2018, Yin *et al.* 2017, Hoek and bray *et al.* 2005, Karatela and Taheri *et al.* 2018). The confined water flow-through structure in those three types of water inrush models can be further divided into three basic water diversion channel types, namely, aquifer, fault fracture zone and fracture zone. In different water inrush types, a water inrush path may consist of one or more water diversion channels. The floor stress state changes under the influence of mining-induced stress. The differential distribution of pore-water pressure in the floor is bound to occur (Huang *et al.* 2014, Hu *et al.* 2014, Kim *et al.* 2018, KUMSAR *et al.* 2000, Lv *et al.* 2019) according to the characteristics of the fluid-structure coupling material. The fault zone generates a dynamic response process under the effect of mining-induced stress. Shear sliding occurs on the fault surface and has a great influence upon material failure in the upper and bottom mass bodies. Changes in the flow characteristics of the fracture zone and fault fracture zone under the effect of mining-induced stress also exert an important influence on the entire water inrush flow process (Yang *et al*. 2007, Wu *et al.* 2003, Yin *et al.* 2011).

In view of the above problems, the nonlinear floor water inrush process has been taken as the research object. Theoretical analysis, laboratory experiments and numerical simulations have been adopted to obtain the stress response characteristics and the coupled flowing law of water flow inside three basic confined water diversion channel types, namely, the aquifer seepage zone, fault zone and fracture zone (Fig. 1) (Yin *et al*. 2017, Zhao *et al.* 2019). The entire process has been analysed, namely, the water flowing from the outside into the aquifer, Darcy's flow in the aquifer, stress-seepage coupled flow in the fault, fracture and other types of broken rock mass, as well as the water flow into the working face (Richard *et al.* 1985, Samanta *et al*. 2018, Varun *et al.* 2017, Wang *et al*. 2016, Wang *et al.* 2019). Thus, the distribution characteristics of water pressure and the time-varying flow velocity law at different stages and

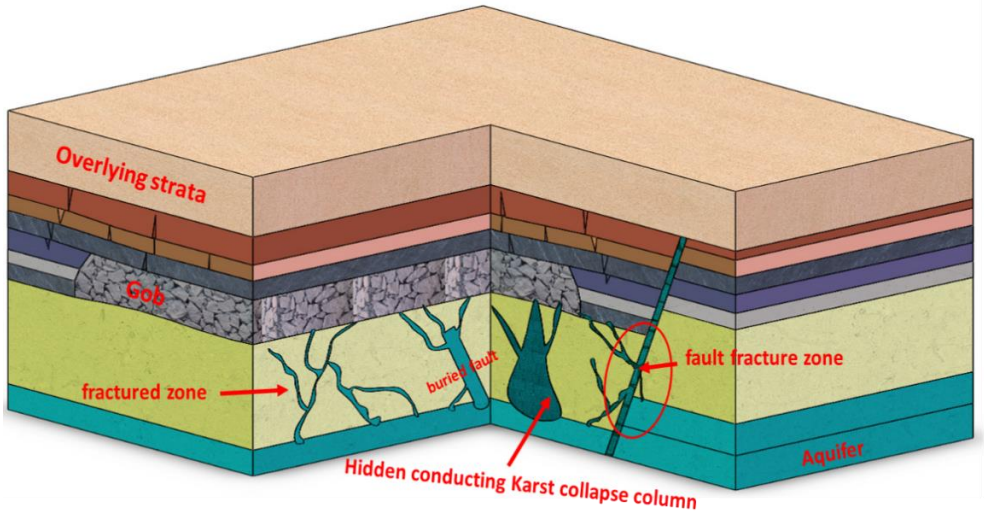

Fig. 1 Floor water inrush mode

time points along the entire water inrush path have been obtained, which offer a reference for corresponding water inflow forecasting and its prevention before and treatment after water inrush.

3. Characteristics of water diversion in aquifer

3.1 Seepage characteristics in aquifer

Floor aquifers, such as strong limestone runoff zones, are one of the main sources of water inrush. Its distribution location is of great significance for forecasting water inrush and its amount (Gao *et al*. 2009, Liu *et al.* 2015). Generally, aquifers are formed in a manner closely related to their geological structure. Faults, fault fracture zones and fracture zones often develop inside an aquifer. It can be a strong runoff zone within a certain area. Therefore, the laws of water enrichment, transport and movement in aquifers serve as a key to forecasting mine inflow. The flow velocity in normal and intact limestone rock masses is small. This is generally known as seepage flow. The hydraulic characteristics of the fractured rock mass contained inside an aquifer and the fluid flow form the fracture flow and even the conduit flow, both of which work as main channels for karst water transport and movement in the aquifer. Karst water flows in a direction basically consistent with that of the geological structure (Wang *et al.* 2018, Xing *et al.* 2007, Xing *et al.* 2000; , Yossff *et al.* 2003, Zhou *et al*. 2020).

Under the influence of fluid-structure interaction, the permeability characteristics of different sedimentary rocks during the process of total stress and strain indicate that the structural changes in internal pores and fissures due to rock deformation are the fundamental reason for changes in rock permeability. The crack-karst network inherently exists in the aquifer, but the fissure network will occur in the floor failure zone under the influence of coal mining disturbance. Once both networks are connected, a complete water diversion channel will be generated, thus increasing mine inflow.

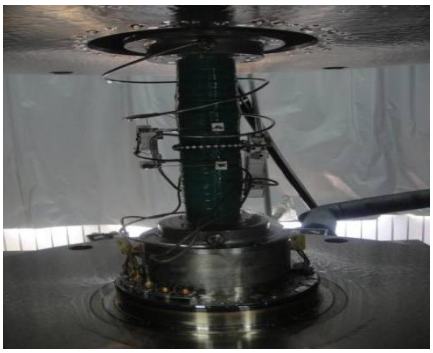

Fig. 2 Permeability Experiment System

3.2 Experimental research on permeability characteristics

Changes to stress in the stope will not only give rise to new fissures but also result in expansion or closure of existing fissures in the rock mass, which will change both permeability and flow velocity and thus cause changes to equivalent stress in the rock mass. The stress state and lithologic characteristics of the rock mass will influence the changing process of the seepage property of the rock mass. As a result, coupling research on stress and pore water pressure must be conducted in light of lithological changes to conform to the actual situation. The total stress–strain-permeability curve of the rock mass can directly exhibit the hydraulic coupling change of the rock mass during the mechanical loading process. Limestone has been adopted for research on seepage characteristics, as shown in Fig. 2. Testing materials were taken from the coalbed floor of the No. 11601 working face in the Geting Colliery. Rock cores were sealed in wax on site immediately after drilling to guarantee the same humidity and moisture content as those on site. After being carried to the laboratory, those rock cores were processed into standard rock specimens (Yin *et al.* 2011, Andric *et al*. 2019, Chen *et al.* 2019a, Chen *et al.* 2019b, Duan *et al.* 2019, Zhao *et al.* 2021). The processed standard rock specimens are cylindrical as required by

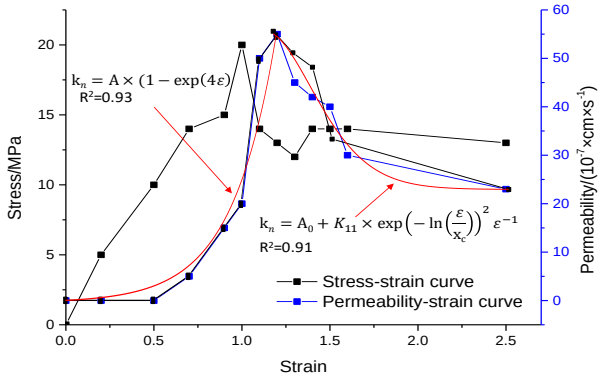

(a) Stress–strain permeability curves of mudstone

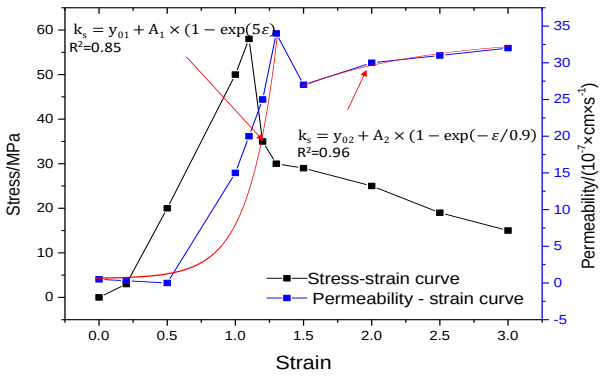

(b) Stress–strain permeability curves of limestone

$$\begin{cases} k = A \times (1 - \exp(4\varepsilon)) & Pre - stress\ Peak \\ y = y0 + K_{11} \times \exp\left(-\ln\left(\frac{\varepsilon}{xc}\right)\right)^2 x^{-1} & Post - stress\ Peak \end{cases} \quad (1)$$

$$\begin{cases} k_s = y_{01} + A_1 \times (1 - exp(5\varepsilon)) & Pre - stress\ Peak \\ k_{sn} = y_{02} + A_2 \times (1 - exp(-\varepsilon/0.9)) & Post - stress\ Peak \end{cases} \quad (2)$$

Fig. 3 Stress–strain permeability curves of mudstone and limestone

specific tests, whose flatness and perpendicularity met the code requirements for testing. The permeability test of the floor rock under high confining pressure was conducted on an MTS815.03 rock servo testing machine, whose sampling, processing and water filling methods are the same as those for the permeability test under low confining pressure. During the testing, the confining pressure was 15 MPa; the pore-water pressures were 4 MPa and 2.5 mPa; and the osmotic pressure difference was 1.5 MPa.

Rock testing can be divided into four stages from loading to failure, namely, the compaction stage, elastic stage, yield stage and postpeak failure stage (Zhang *et al.* 2016, Zhao *et al.* 2019). Rock mass permeability can be divided into the prior and post stages according to the stress peak location. During the initial stage of loading, the pores and fissures inside the rock gradually close, and its permeability decreases temporarily. With increasing axial stress, the specimens are compressed further. The formation of new fractures and the expansion of original fractures can result in an increasing permeability in those specimens. As the axial pressure continues to increase, the internal damaged increases, and the fractures expand more. When reaching the stress peak, the new fractures and the original fractures begin to connect and form a fracture network, thus causing a drastically increased permeability, as shown in Fig. 3. (Yuan *et al.* 2019).

where parameter $A = -0.46$, $A_0 = 23, K_{11} = 282, x_c = 1.3$; $A_1 = -0.05$, $y_{01} = 0.5$, $A_2 = 32.16$, $y_{02} = 1$; k_s is the prepeak permeability coefficient of mudstone; and k_{sn} is the postpeak permeability coefficient.

During the late stage of the stress peak, the fractures in the rock mass gradually change from isolated deformation and slippage to joint slippage failure. The fissure tips begin to crack and extend into the adjacent fissures. The rock undergoes volumetric expansion and deformation, so its permeability further increases. Although limestone specimens do not enter the plastic flow state after the peak, they demonstrate obvious plastic characteristics. Under the effect of high confining pressure, the internal fractures are closed to a certain extent, so their permeability undergoes a certain degree of reduction. However, it remains at a high level. A great number of microcracks expand and then form a macroscopic fractured surface. The slope of the curve is negative and changes gradually as the strain increases. The holistic stress structure of the rock is lost. The volume of the internal intact carrier is gradually segmented and weakened as the fractures expand, presenting a discontinuous state. The local permeability decreases and this ultimately influences the change in permeability of the water-diverting rock mass (such as limestone) after different peaks.

According to Fig. 3, the permeability of the rock mass is not fixed but changes gradually as the stress value increases. Therefore, it is not accurate to generalize those flowing movements in the aquifer using Darcy's law. Instead, the stress level of the rock mass should be determined according to the actual mining situation to precisely obtain the seepage flow characteristics inside the rock mass. In the figure, exponential functions can be adopted to represent the limestone status before and after the peak, and both are increasing functions. However, there is a short declining stage during the transition before and after the peak. The differences in transition permeabilities among rocks with different rock characteristics before and after the peak are large. Therefore, water inflow forecasts should be categorized according to the lithology and the stress state.

4. Water diverting characteristics of the fracture zone

4.1 Geometric characteristics of joint fissures in rock mass

Joint apertures are the most basic parameters used to depict the geometrical characteristics of permeable joint planes. They all have important influences on the seepage characteristics and mechanical properties of permeable joint

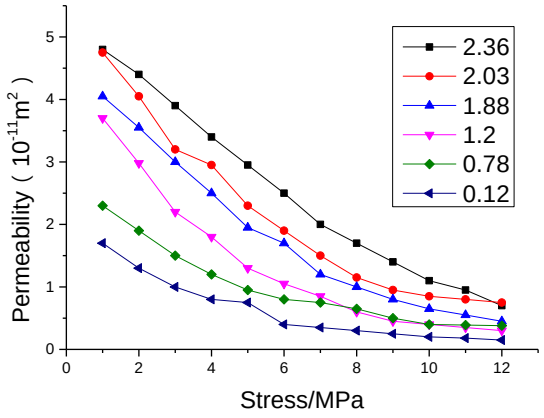

Fig. 4 Permeability of specimens in different loading and surface roughness

planes. According to different determination methods, joint apertures can be defined as the geometrically measured mechanical aperture, maximum mechanical aperture (E_{max}) and hydraulic equivalent aperture. According to the research, the three aperture values are the same for smooth and parallel plate fractures, but they are usually different for realistic rough fractures. During the loading and unloading process, due to the friction on the joint wall and the zigzagging and bending of the joint surface, the mechanical aperture E of a realistic irregular joint is larger than the hydraulic aperture e of an ideal parallel plate. That is, a smooth fracture has a smaller aperture than a rough fracture under the condition of the same hydraulic diversion capacity (Zhao *et al.* 2018a, Yang *et al.* 2019). During coal mining, it is impossible to obtain the initial conditions for fracture propagation and the propagation mechanism and law under the effect of water flow on site. These data can only be obtained through simulation experiments in the laboratory based on the comprehensive consideration of the physical and mechanical properties of rock, the fissure state and the flow parameters. Therefore, the fissure inflow and propagation law have been explored herein in terms of the dynamic process of water inflow, variation characteristics of water pressure and water inflow, and fracture propagation degree.

4.2 Experimental research on the seepage characteristics of joint fractures in a rock mass

Fracture seepage experiments on two groups of rock specimens with different rough surfaces were conducted through the establishment of different water injection pressures and crack widths, as shown in Fig. 4. (Sun *et al.* 2016, Zhang *et al*. 2017) to obtain the variation rules of the water pressure in the experimental aquifer and the water inflow via the fracture channel. The influences of the water injection pressure, crack width and roughness of the fracture surface on the fracture propagation of weathered mudstone are discussed. Then, the seepage laws in fractures on the rough surface of the rock mass under the effect of water flow are summarized.

According to the literature (Sun *et al.* 2016), the rough-surface permeability in a fractured rock mass can be expressed as

$$k_r = y_{03} + 2A_3 \times \left(1 - exp\left(-\frac{x}{t_1}\right)\right) \quad (3)$$

where

$$y_{03} = 5.46 + \frac{-3.27}{1 + \left(\frac{J}{0.96}\right)2.95}$$

$$A_3 = -2.07 + 0.44 \times \left(1 - exp\left(\frac{J}{0.9}\right)\right)$$

$$t_1 = 3.55 - 0.0063 \times \left(1 - exp\left(\frac{J}{3.29}\right)\right)$$

where J is the absolute roughness of the fracture surface and X is the normal load. When there are multiple fractures, the total fracture aperture H can be calculated through the superposition principle.

$$H = \sum_{i=1}^{n} J_i \quad (4)$$

where n is the fracture number and J_i is the roughness of each fracture.

Therefore, the maximum seepage flow from the multifractured rock mass can be expressed as

$$k_{max} = \sum_{i=1}^{n} k_i \quad (5)$$

where k_i is the permeability of each fracture.

Generally, it is difficult to directly measure the fracture density of a rock mass. However, the density (frequency) and the aperture of fractures can be calculated from the RQD values obtained during drilling. The fracture frequency in the rock mass can be obtained according to the relationship between the RQD and structural plane frequency as established by Priest and Hudson (Hudson and Harrison 1997, Priest and Hudson 1976)

$$QD = 100(1 + 0.1\lambda)e^{-0.1\lambda} \quad (6)$$

where λ is the structural plane frequency.

RQD is actually a vector-like quantity with both magnitude and direction. However, one can apply the RQD obtained from vertical drilling to other directions to approximate both the upper and lower limits of the total permeability coefficient and to apply both to mine inflow forecasting.

5. Water diverting characteristics of the fault fracture zone

5.1 Experimental devices for determining the water diverting characteristics of the fault fracture zone

The fault fracture zone is generally filled with gravel, whose internal flow characteristics are critical to knowing the flow process of water inrush from the fault (Li *et al.* 2019, Lu *et al*. 2015,; Mandal *et al.* 2019, Munoz et al. 2016). Therefore, the self-developed experimental system for crushed rock deformation and seepage has been adopted to conduct simulation research on stress and seepage. The experimental machine and specimens are shown in Fig. 5 (Zhao *et al.* 2018).

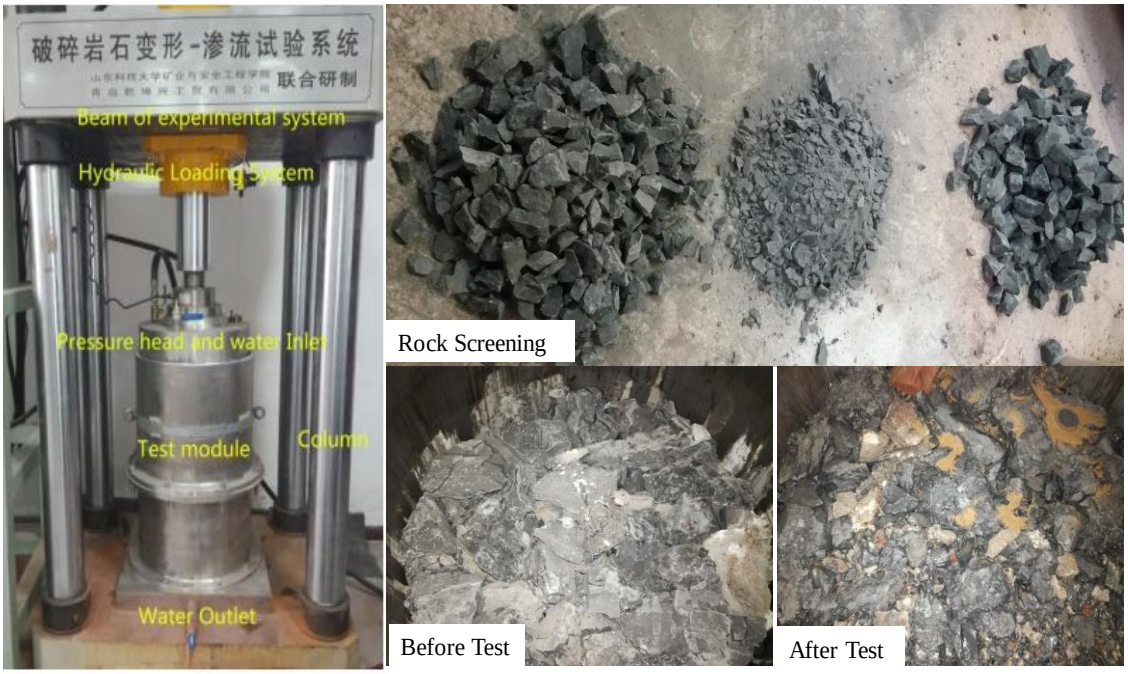

Fig. 5 Rock Screening and Experimental Process

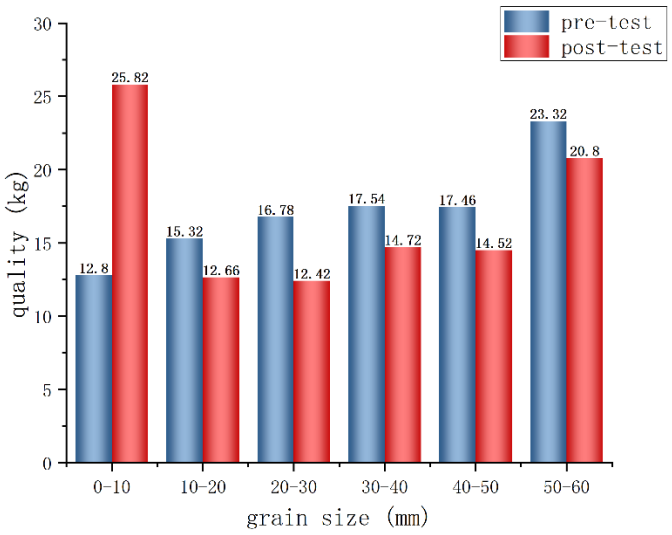

Fig. 6 Different particle sizes before the test

The experimental compaction head is made of a 20-mm thick plate of bearing steel, with an internal load-bearing frame to increase its resistance to deformation. The water pressure of the experimental control system and the stress loading system are independent from each other to realize real-time monitoring and data acquisition concerning displacement, load, water pressure and water volume. The maximum water pressure is 2 MPa, and the precision is 0.01 MPa. The particle size of broken rock in natural state and saturated state after test is re-screened and weighed. The comparison of the quality changes of broken rocks with different particle sizes before and after is shown in Table 1 and Figs. 6 and 7 (Kong 2017). The comparison results pre and post the test show that with the stress loading, the rock mass particles decrease, and the proportion of rock mass particles with particle size less than 40 mm increases from 45.23% to 63.58%. However, with the loading of water pressure, the particle loss of rock medium increases, and the final particle loss reaches 2.98 KG. The maximum axial loading force is 600 kN, and the accuracy is 0.01 kN. The stress seepage coupling process of gravel with different particle sizes has been researched herein under different stresses. The findings show that the particle size plays a major role in permeability under the same stress state when

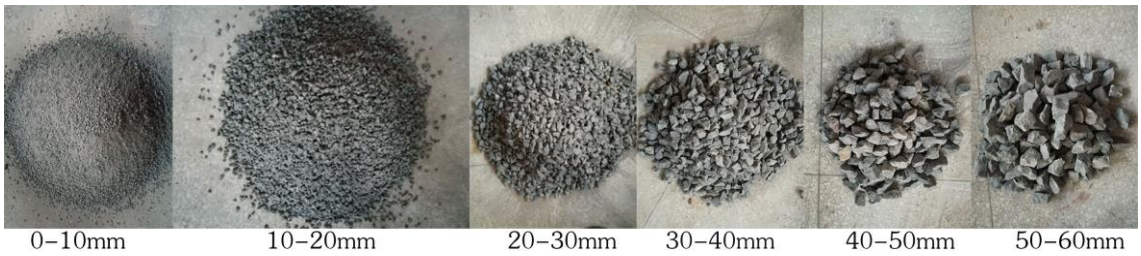

Fig. 7 Different particle sizes before the test

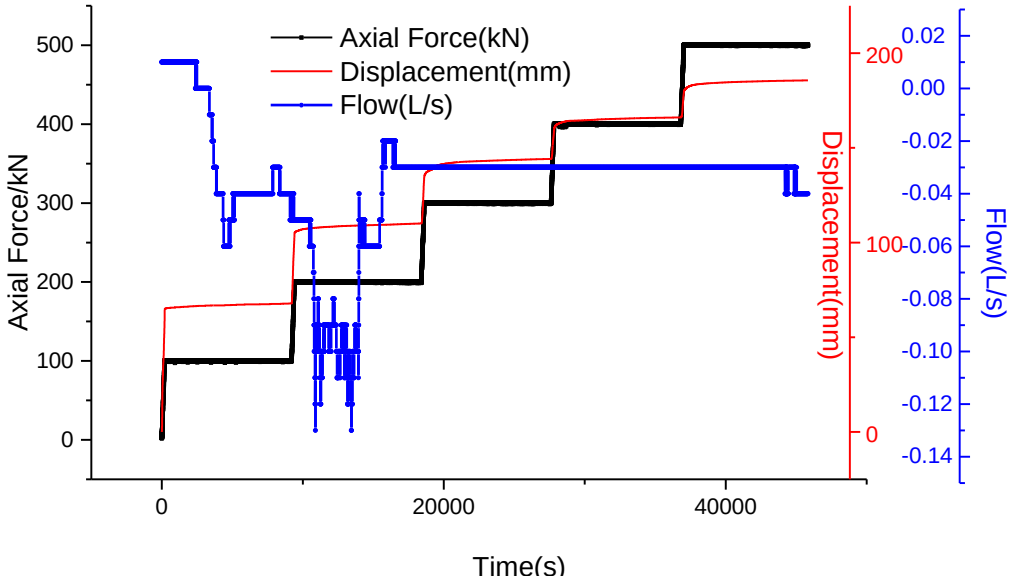

Fig. 8 Curve of Influence from Different Axial Forces on Average Flow

Table 1 Quality changes of broken rock with different particle sizes

Particle size / mm	0~10	10~20	20~30	30~40	40~50	50~60	Total mass / kg
Pre-test	12.80	15.32	16.78	17.54	17.46	23.32	103.22
Post-test	25.82	12.66	12.42	14.72	14.52	20.80	100.94

the stress is small; the permeability of the rock mass increases with particle size; the gravel body is compacted and the fracture space is reduced when the stress increases, and the influence of particle size on permeability is reduced; when the stress is above 400 kN, the stress plays a dominant role in the permeability of gravel while the effect of particle size on permeability decreased.

5.2 Experiment on the water diverting characteristics of the fault fracture zone

The relationship between particle size-stress and permeability is shown in Fig. 8. Rock blocks with particle sizes ranging from 5 to 10 cm were selected for experimental research. The axial force was loaded by the graded loading method from 100 kN to 500 kN, using five loading stages with a loading rate of 0.5 kN/s. After the set pressure has been met, the load was kept unchanged, and the duration of each dead load stage lasted 2500 s to conduct the seepage experiments under the same stress conditions and different water pressure conditions.

Under the effect of the same load, the water pressure is loaded up to the set value, and the axial load and the end water pressure remained unchanged. Then, the drainage valve was opened for the seepage test. Since the feed water flow rate of the experimental machine was small, the water discharge time was set at 5 s herein to eliminate the influence of discontinuous water flow inside the gravel body on the experimental results. The drainage valve was closed after the monitoring task was completed. Water pressure was then continued and water was loaded int preparation for another water pressure stage. The above steps were repeated for the experiment. The monitoring results were cross-verified by manual and software recording. To ensure the accuracy of the experimental results, no water flow interruption occurred during the experiment. The relationship between the hydraulic gradient and flow velocity is nonlinear.

The Forchheimer equation was adopted to fit the formula of water pressure and seepage velocity monitored at the outlet (Fig. 9 and Table 2). The seepage law in a gravel body is (Zhao *et al.* 2018b, Sweetenham *et al.* 2017)

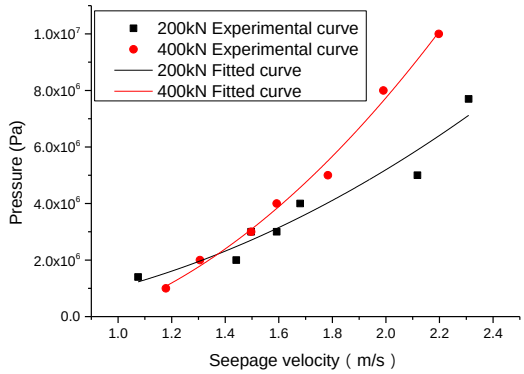

Fig. 9 Comparison of the Forchheimer Simulation Results and the Experimental Values

Table 2 Fitting Parameters of the Forchheimer Equation

Equation	$J = av + bv^2$	
200 kN	A	5.46×105
	B	1.57×106
400 kN	A	3.32×106
	B	3.60×106

$$J = av + bv^2 \qquad QD = 100(1 + 0.1\lambda)e^{-0.1\lambda} \qquad (7)$$

where the coefficient is expressed as: $J = \partial p/\partial x$, $a = -\mu/\rho K$ and $b = -\beta\rho$. The fitting parameters herein are A=6.33 and b=4.78. The physical meanings of each parameter in the formula are μ is the fluid viscosity coefficient (kg/(m×s)), ρ is the fluid density, β is the non-Darcy influence coefficient, and g is the gravitational acceleration. According to the experimental results, the flow process meets the realistic experimental law. Under the condition of laminar flow, the second term bv^2 in Eq. (7) can be ignored, in which case the Forchheimer equation is actually Darcy's law.

6. Coupling flow characteristics among different water diversion channels

Before the formation of the water inrush channel, the flow velocities of the fluid in the aquifer, the fault and the broken rock mass are low, and their resistance is mainly the linear friction force. Therefore, Darcy's law can be adopted to determine an approximate solution. After entering the stope or channel, the liquid flow obeys the free Navier–Stokes equation. The fluid density in saturated porous media in the aquifer can be considered to be constant. When there is sufficient water supply in the aquifer, the floor interface of the aquifer can be treated as the constant water pressure boundary. When the flow in the aquifer is constant, the floor interface of the aquifer can be regarded as the boundary with constant velocity (Yang *et al.* 2017, Gao *et al.* 2009, Tatone *et al*. 2015).

After the formation of the water inrush channel, the permeability coefficient in the fault fracture zone increases sharply. When the water volume in the aquifer is sufficient and when the medium in the aquifer is subjected to a smaller influence from changes in stress, the fluid flow in the aquifer still meets Darcy's law. However, the Forchheimer equation, dominated by the momentum equation, should be adopted as the main controlling equation when the flow velocity increases significantly in the fault and fractured rock mass. The fluid meets the boundary conditions of equal water pressure and equal velocity (Yang *et al.* 2017, Yao *et al.* 2018, Wu *et al.* 2019, Zhang *et al*. 2015) at the aquifer-fault, fault–fractured rock mass, and fractured rock mass-channel interfaces.

7. Case analysis

Numerical simulation analysis and verification were conducted against the backdrop of water inflow changes in a mine in Shandong province to verify the rationality of mine inflow forecasting by RQD parameters. The working face in this mine is 240 m in length and 140 m in dip length, with a mining depth of 70 m (Zhao *et al.* 2022). The working face is located in a water enrichment area with karst fissure development. The direct aquifer is Xujiazhuang limestone (Limestone 5) of the Benxi Formation, with a thickness of 12.24 m and a water level of 20 m. It is only approximately 12.5 m away from the Ordovician Limestone and has a close hydraulic connection to the Ordovician limestone. The Ordovician limestone aquifer is approximately 800 m thick and rich in water. It is the main replenishment water source of the Ordovician limestone. The numerical model established upon geological conditions is displayed in Fig. 8. The aquifuge from the coal floor to Limestone 5 (Aquifer) mainly consists of clay rock and siltstone and has a thickness of approximately 16.5 m. The working face is located in the strong limestone runoff zone. Influenced by the destruction of the coal floor induced by coal mining, the risk of water inrush from the coal floor is high, with a water inrush probability greater than 95%.

The numerical simulation of solid mechanics-Darcy 's law-Brinkman fluid-solid coupling field is adopted. The thickness of the coal seam is 6 m. The bottom of the model is fixed to restrict the movement up and down. Rod support is applied on both sides to restrict the movement left and right, and the overlying strata load is applied on the top 25 MPa. The aquifer water pressure is 10 MPa, and the goaf is atmospheric pressure. The fracture of the floor rock mass is developed, and the collapse column is located in the footwall of the fault(Fig. 10). The parameters of each rock layer are shown in Table 3.

Fig. 11 show the distribution characteristics of the pore-water pressure on the stope when the RQD values of the floor rock mass are 93,76,44 and21, respectively. According to these figures, the stress distribution of the original rock has been destroyed due to the influence induced by mining. Therefore, the permeability in the rock mass changed greatly and thus it impacts the changes in the flow path and flow state in the aquifer. As a result, a pressure relief zone is

Table 3 Mechanical properties of rock stratums

Rock formation	ρ(kg/m3)	E(GPa)	v	φ	μ(Pa . s)	K(m^2)
sandy mudstone	2700	20	0.25	0.05	0.001	1×10^{-13}
Coal	1400	10	0.28	0.1	0.001	3×10^{-13}
mudstone	2600	20	0.25	0.08	0.001	1×10^{-14}
Aquifer	2700	18	0.26	0.2	0.001	1×10^{-12}
Fault	2000	5	0.3	0.2	0.001	1×10^{-9}
Collapse column	2200	0.5	0.3	0.3	0.001	1×10^{-8}

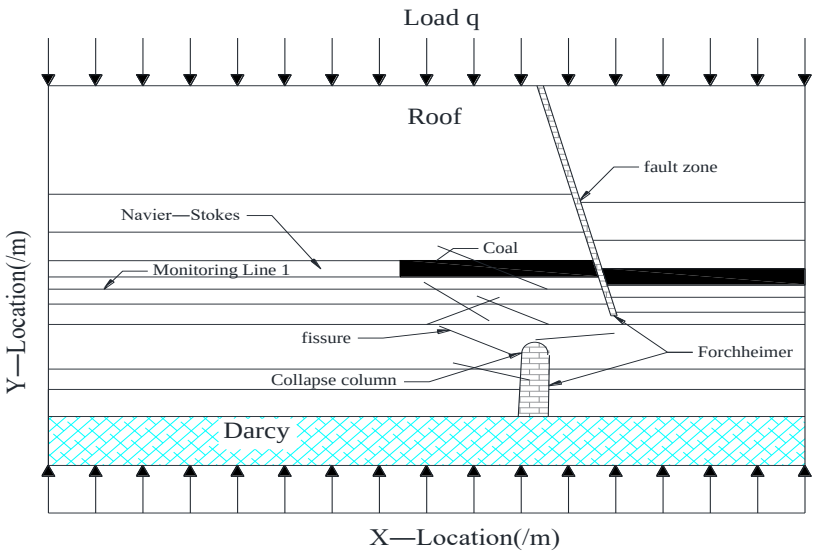

Fig. 10 Diagram of Calculation Model

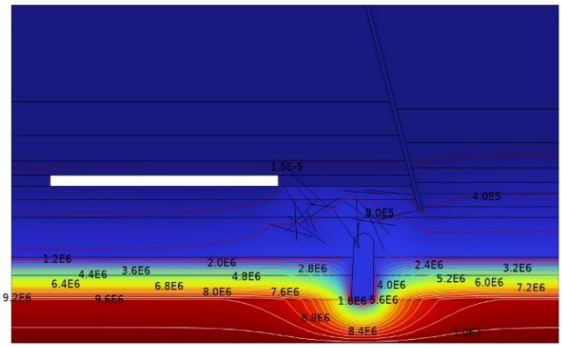

(a) Water Pressure Distribution with an RQD value of 93(Pa)

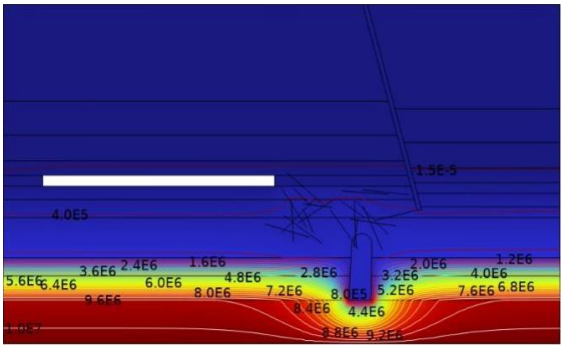

(b) Water Pressure Distribution with an RQD value of 76

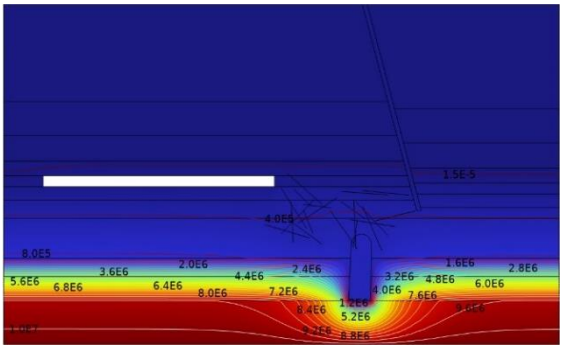

(c) Water Pressure Distribution with an RQD value of 44

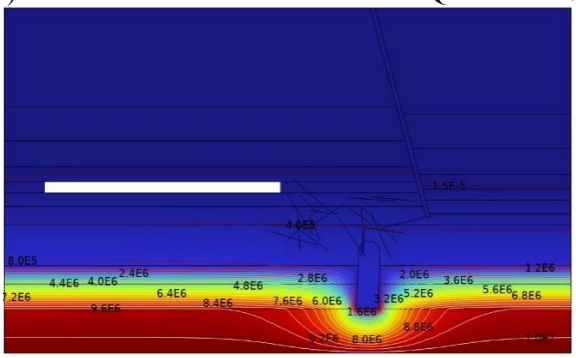

(d) Water Pressure Distribution with an RQD value of 21

Fig. 11 Characteristics of the pore water pressure distribution in the mining floor with different RQD values

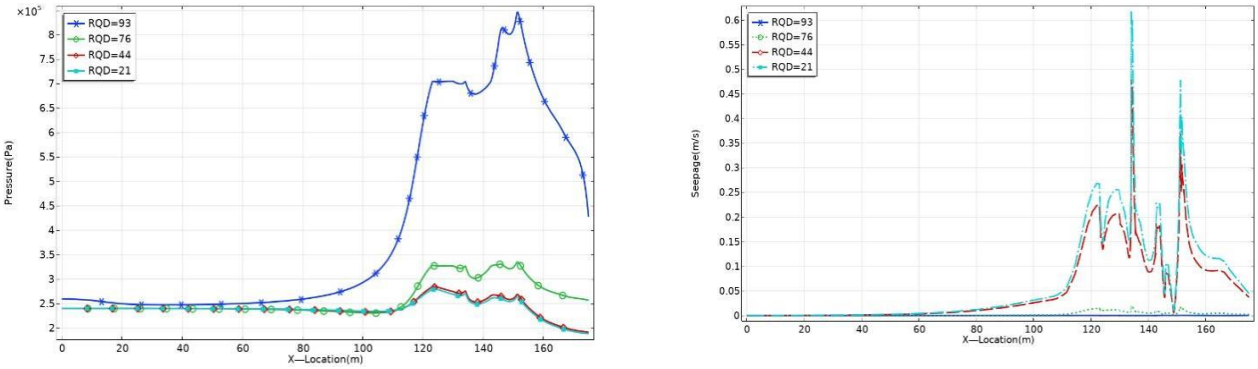

(a) Pore water pressure (b) Seepage distribution

Fig. 12 Pore water pressure and Seepage distribution of monitoring1 with different RQD values

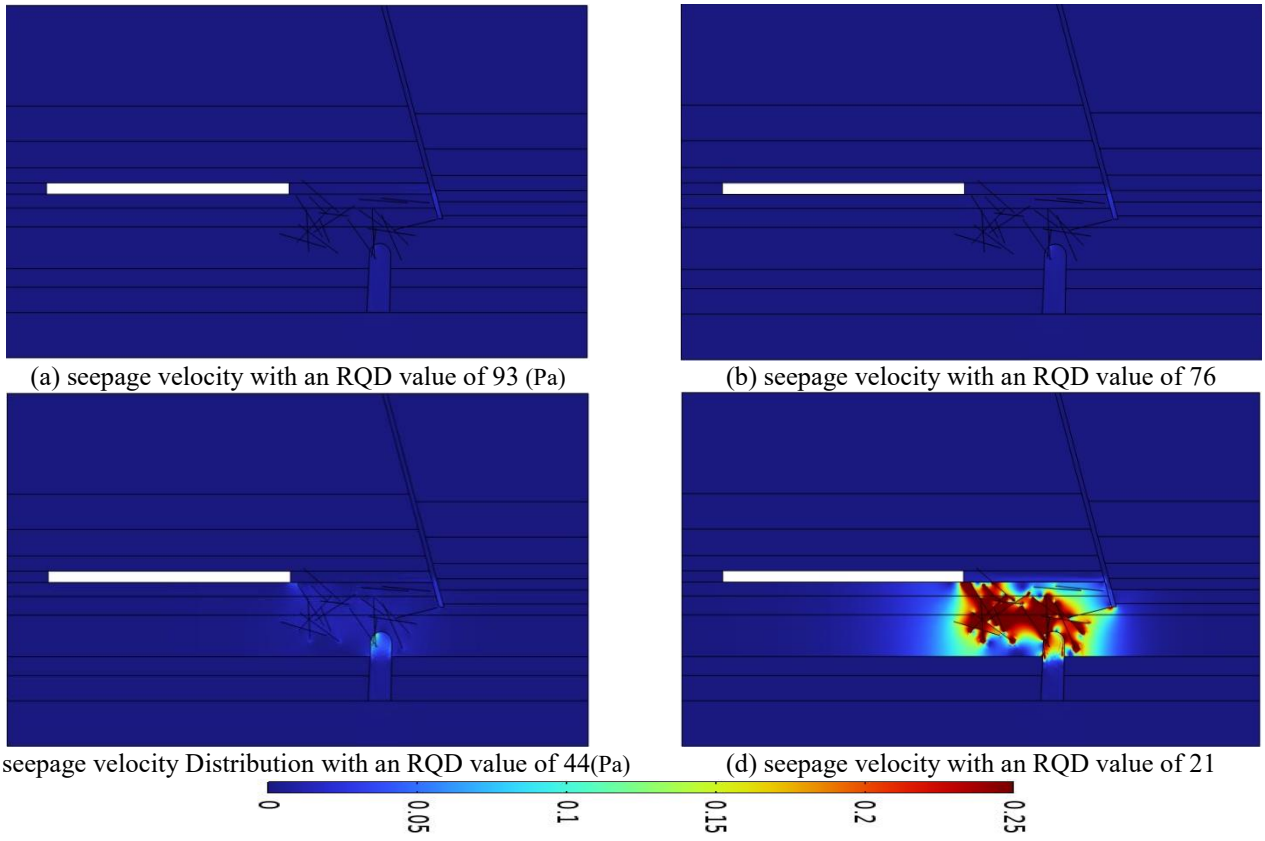

(a) seepage velocity with an RQD value of 93 (Pa) (b) seepage velocity with an RQD value of 76

(c) seepage velocity Distribution with an RQD value of 44(Pa) (d) seepage velocity with an RQD value of 21

Fig. 13 Seepage velocity of mining floor with different RQD values

formed near the mining face, It can be shown from the change curve of pore water pressure corresponding to different RQD values on Monitoring Line 1 in Fig. 12 that with the decrease of RQD values, the pore water pressure in front of the coal working face decreases.

According to Fig. 13, with the decrease of RQD value of rock mass, the fragmentation of rock mass increases, and the fracture develops and penetrates, forming a seepage channel between collapse column-floor-fault, resulting in a sharp increase in water inflow in goaf.

As the RQD value of the rock mass decreases, the frequency of the fracture surface in the rock mass increases, the rock mass breaks even more, and the water inflow into the goaf increases. Therefore, the pore-water pressure value in the stope also decreases. Such a change process is the same as that of water pressure monitoring during the realistic mining process. As the overall RQD index of the rock mass in the mine increases, the mine inflow also increases rapidly. This indicates that the more broken the rock mass is, the greater the daily water inflow value of the coal mine is. As the RQD value tends to be 100, the mine inflow tends to be 0. According to Figs. 14 and 15, when affected by a fault, the confined water is mainly subject to water diversion in the fault. However, changes in the RQD value of the rock mass have a smaller influence on mine inrush. At this moment, the calculation of fault inflow

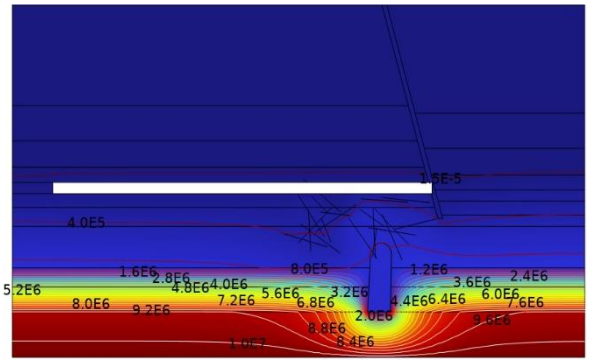

(a) Water Pressure Distribution with an RQD value of 93 (Pa)

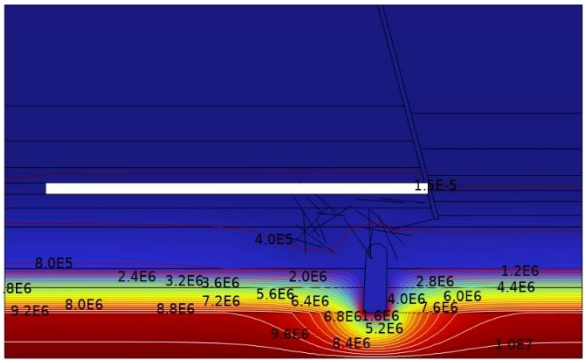

(b) Water Pressure Distribution with an RQD value of 76

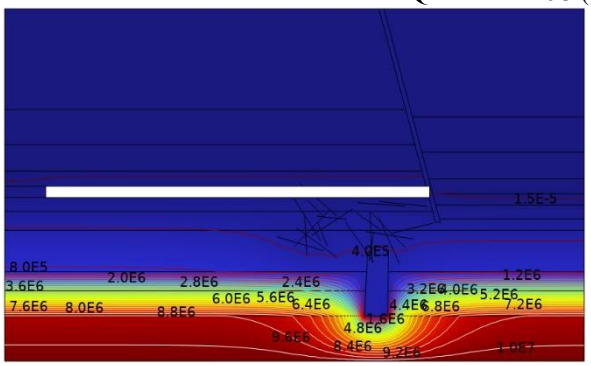

(c) Water Pressure Distribution with an RQD value of 44(Pa)

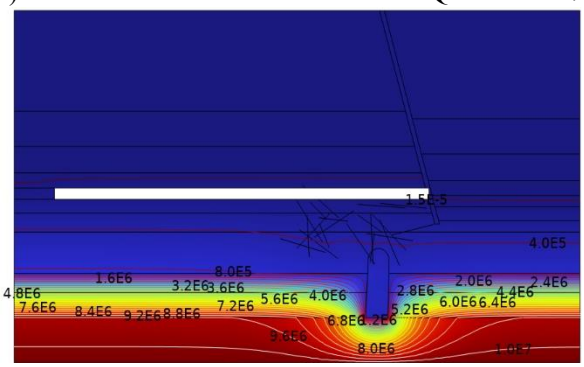

(d) Water Pressure Distribution with an RQD value of 21

Fig. 14 Characteristics of the pore water pressure distribution in the mining floor with different RQD values

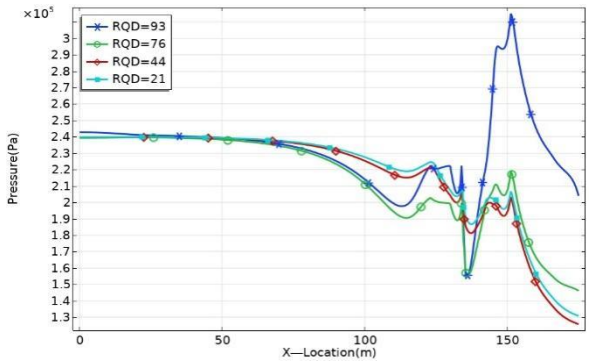

(a) Pore water pressure

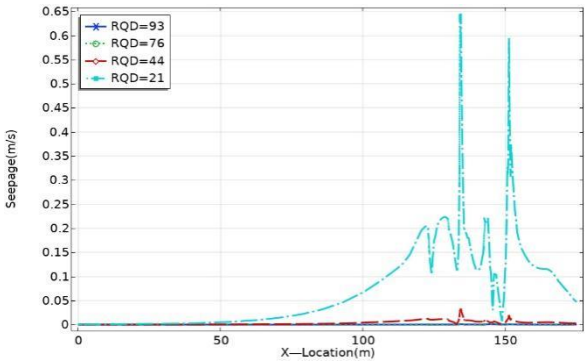

(b) Seepage distribution

Fig. 15 Pore water pressure and Seepage distribution of monitoring1 with different RQD values

should be considered the critical aspect that conforms to the realities. According to Fig. 16, with the decrease of RQD value of rock mass, the fragmentation of rock mass increases, and the fracture develops and penetrates, forming a seepage channel between collapse column-floor-fault, resulting in a sharp increase in water inflow in goaf. At the same time, when the coal seam passes through the fault, the seepage channel of the floor increases and the high seepage area increases.

8. Conclusions

- According to the traditional qualitative analysis method that determines the probability of water inrush based on stratum structure, the water inrush types have been divided into aquifer, fracture zone and fault fracture zone according to the characteristics of the water diversion channel. The flow laws of the water in those three water diverting bodies have been obtained experimentally. The coupling flow effect of the fluid between water diversion channels has been analysed in a quantitative manner. It has been noted that the water-diverting path and law can be summarized by those three types of water diversion channels.
- The relationship equation between the RQD index and permeability in a multifractured rock mass has been established by virtue of the relationship between RQD and fracture frequency and in light of the characteristics of seepage flow in the fractures on the rough surface. The equation has been verified by numerical simulation. The equation establishes the

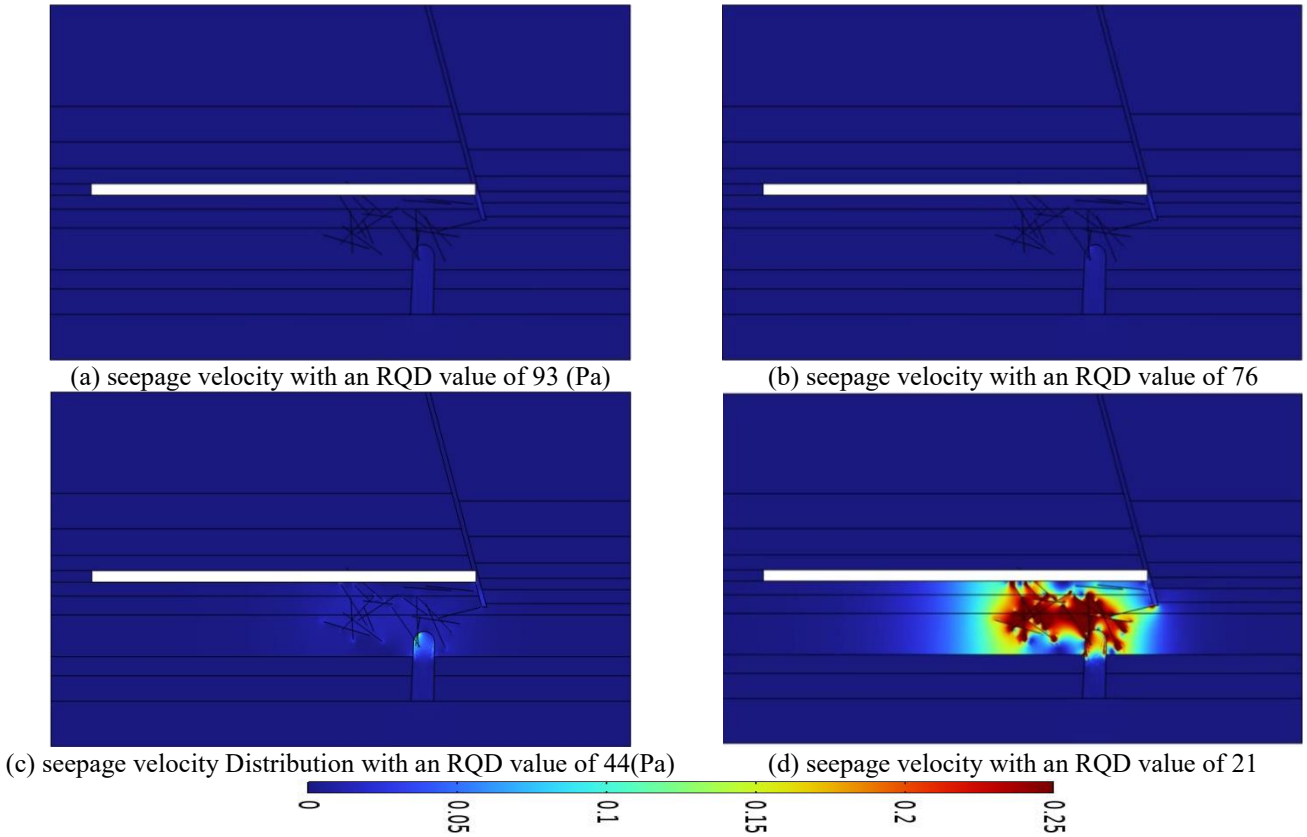

(a) seepage velocity with an RQD value of 93 (Pa)
(b) seepage velocity with an RQD value of 76
(c) seepage velocity Distribution with an RQD value of 44(Pa)
(d) seepage velocity with an RQD value of 21

Fig. 16 Seepage velocity of mining floor with different RQD values

correlation between the theoretical analysis and practical engineering application. Therefore, it is of great significance to water inflow forecasting during practical engineering.

- The results of this study provide a new theoretical basis and technical method for the mechanism and prevention of mine water inrush, which has important scientific significance. In the future, based on this research method, we can further deepen the detailed study of mine water inrush path, improve the accuracy of water inrush prediction, and promote the development of mine water disaster prevention and control technology. At the same time, the multi-structure coupling flow model and the concept of water inrush intensity proposed in this study also provide a reference for disaster prediction and prevention in other similar fields, and have broad application prospects. In general, this study not only enriches the theoretical system of mine water inrush, but also provides important technical support for practical engineering applications and promotes the development of mine safety production.

Acknowledgments

Funding was provided by the National Natural Science Foundation of China (52104203); Shandong Province Natural Science Foundation Project (ZR2020QE128; ZR2020ME102; ZR2021ME138); National Key R&D Program of China (2018YFC0604705); SDUST Research Fund (grant 2018TDJH102).

References

Adhikary, D. (2012), "Numerical simulation of mine water inflow", *Proceedings of the international society for rock mechanics*, Stock-holm, Sweden. https://www.onepetro.org/conference-paper/ISRM-EUROCK-2012-0

Andric, P., Yin, B. and Curtin, W.A. (2019), "Solids Physics of Stress-dependence of generalized stacking fault energies", *J. Mech. Phys. Solids*, **122**, 262-279. https://doi.org/10.1016/j.jmps.2018.09.007.

Battumur (2009), "Assessment of water supply options for proposed bayan airag gold-copper mine", Report: January 2009.

Blum, P., Mackay, R., Riley, M.S., Finkel, M., Barcelo, D., Barth, J.A.C. and Grathwohl, P. (2009), "Stochastic simulations of regional scale advective transport in fractured rock masses using block upscaled hydro-mechanical rock property data", *J. Hydrology*, **369**(3), 318-325 https://doi.org/10.1016/j.jhydrol.2009.02.009.

Bouzourra, H., Bouhlila, R., Elango, L., Slama, F. and Ouslati, N. (2015), "Characterization of mechanisms and processes of groundwater salinization in irrigated coastal area using statistics, GIS, and hydrogeochemical investigations", *Environ Sci. Pollut. Res.*, **22**(4), 2643-2660. https://doi.org/10.1007/s11356-014-3428-0.

Chen, Y., Jiang, C., Yin, G., Zhang, D., Xing, H. and Wei, A. (2019b), "Permeability evolution under true triaxial stress conditions of Longmaxi shale in the Sichuan Basin", *Southwest*

China. Powder Technol., **354**, 601-614. https://doi.org/10.1016/j.powtec.2019.06.044.

Chen, Y., Lian, H., Liang, W., Yang, J., Nguyen, V.P. and Bordas, S.P.A. (2019a), "The influence of fracture geometry variation on non-Darcy flow in fractures under confining stresses", *Int. J. Rock Mech. Min. Sci*., **113**, 59-71. https://doi.org/10.1016/j.ijrmms.2018.11.017

Chen, Y., Zhu, S.Y., Yang, C.W. and Xiao, S.J. (2021b), "Analysisof hydrochemical evolution in main discharge aquifers under mining disturbance and water source identification", *Environ. Sci. Pollut. Res*., **28**, 26784-26793. https://doi.org/10.1007/s11356-021-12639-w.

Duan, M., Jiang, C., Gan, Q., Li, M., Peng, K. and Zhang, W. (2019), "Experimental investigation on the permeability, acoustic emission and energy dissipation of coal under tiered cyclic unloading", *J. Nat. Gas Sci. Eng*., https://doi.org/10.1016/j.jngse.2019.103054.

Gao, Y.F., Zhang, Y.P., Zhang, H.M. and Wang, S.F. (2009), "Research on expert system for risk assessment of water inrush from coal floor and its application", *Chinese J. Rock Mech. Eng*., **28**(2), 253-258.

Ghyasvand, S., Fahimifar, A. and Nejad, F.M. (2022), "On the optimum design of reinforcement systems for old masonry railway tunnels", *Geomech. Eng*., **28**(2), 145-155. https://doi.org/10.12989/gae.2022.28.2.145.

Goodman, R.E. and Shi, G. (1985), "Block theory and its application to rock engineering", Englewood Cliffs, New Jersey: Prentice-Hall.

Gu, Q.X., Huang, Z., Li, S.J., Zeng, W., Wu,Y. and Zhao, K. (2020), "An approachfor water-inrush risk assessment of deep coal seam mining: a case study in Xinlongzhuang coal mine", *Environ. Sci. Pollut. Res*., **27**(34), 43163-43176. https://doi.org/10.1007/s11356-020-10225-0.

Guo, W.J., Zhang, S.C., Sun, W.B. and Chen, J.T. (2018), "Experimental and analysis research on water inrush catastrophe mode from coal seam floor in deep mining", *J. China Coal Soc*., **1**, 219-227. https://doi.org/10.13225/j.cnki.jccs.2017.0774.

Hasiniaina, F., Zhou, J. and Guoyi, L. (2010), "Regional assessment of groundwater vulnerability in Tamtsag Basin", Mongolia using drastic model", *J. Am. Sci*., **6**(11), 65-78

Hoek, E. and Bray, J.W. (2005), "Rock slope engineering", 4th Ed., New York: Spon Press.

Hou, W., Cao, S. and Gao, X. (2016), "Study on water enrichment detection and water inrush of top slate rock layer in the first mining surfaceof Xin'an Coal Mine", *China Min*., **25**(2), 270-272.

Hu, X., Wang, L., Lu, Y. and Yu, M. (2014), "Analysis of insidious fault activation and water inrush from the mining floor", *Int. J. Min. Sci. Technol*., **24**(4), 477-483. https://doi.org/10.1016/j.ijmst.2014.05.010.

Huang, Z., Jiang, Z., Zhu, S., Qian, Z. and Cao, D. (2014), "Characterizing the hydraulic conductivity of rock formations between deep coal and aquifers using injection tests", *Int. J. Rock Mech. Min. Sci*., **71**, 12-18. https://doi.org/10.1016/j.ijrmms.2014.06.017.

Huang, Z., Zeng, W. and Zhao, K. (2019), "Experimental investigation of the variations in hydraulic properties of a fault zone in Western Shandong", *China. J. Hydrol*., **574**, 822-835.

Hudson, J.A. and Arrison, J.P. (1997), "Engineering rock mechanics", [S.l.]: Pergamon.

Ibishi, G.; Genis, M. and Yavuz, M. (2022), "Post-pillars design for safe exploitation at Trepca hard rock mine (Kosovo) based on numerical modelling", *Geomech. Eng*., **28**(5), 463-475. https://doi.org/10.12989/gae.2022.28.5.463.

Karatela, E. and Taheri, A. (2018), "Three-dimensional hydro-mechanical model of borehole in fractured rock mass using discrete element method", *J. Nat. Gas Sci. Eng*., **53**, 263-275. https://doi.org/10.1016/j.jngse.2018.02.032.

Khorasani, E., Amini, M., Hossaini, M.F. and Medley, E. (2019), "Evaluating the effects of the inclinations of rock blocks on the stability of bimrock slopes", *Geomech. Eng*., **17**(3), 281-287. https://doi.org/10.12989/gae.2019.17.3.281.

Kim, E., Garcia, A. and Changani, H. (2018), "Fragmentation and energy absorption characteristics of Red, Berea and Buff sandstones based on different loading rates and water contents", *Geomech. Eng*., **4**(2), 151-159. https://doi.org/10.12989/gae.2018.4.2.151.

Komurlu, E., Kesimal, A. and Demir, S. (2016), "Experimental and numerical analyses on determination of indirect (splitting) tensile strength of cemented paste backfill materials under different loading apparatus", *Geomech. Eng*., **10**(6), 775-791. https://doi.org/10.12989/ gae.2016.10.6.775.

Kong, D.Z. (2017), Study on activation and instability of overlying rock mass in old goaf under load .Shandong University of Science and Technology.

Kumsar, H., Aydan, O. and Ulusay, R. (2000), "Dynamic and static stability assessment of rock slopes against wedge failures", *Rock Mech. Rock Eng*., **33**(1), 31-51. https://doi.org/10.1007/s006030050003.

Lawal, A.I.; Kwon, S., Aladejare, A.E. and Oniyide, G.O. (2022), "Prediction of the static and dynamic mechanical properties of sedimentary rock using soft computing methods", *Geomech. Eng*., **28**(3), 313-324. https://doi.org/10.12989/gae.2022.28.3.313.

Li, B. and Wu, Q. (2019), "Catastrophic evolution of water inrush from a water-rich fault in front of roadway development: A case study of the Hongcai coal mine", *Mine Water Environ*., **3**, 1-10. https://doi.org/10.13199/j.cnki.cst.2019.12.024.

Liu, S.L., Li, W.P. and Wang, Q.Q. (2017), "Height of the water-flowing fractured zone of the Jurassic coal seam in northwestern China", *Mine Water Environ*., **37**(2), 312-321. https://doi.org/10.1007/s10230-017-0501-1.

Liu, W., Liu, S. and Liao, S.H..(2015), "Study on water inrush passage from floor affected by fault", *Coal Eng*., **12**, 85-88.

Lu, Y. and Wang, L. (2015), "Numerical simulation of mining-induced fracture evolution and water flow in coal seam floor above a confined aquifer", *Comput. Geotech*., **67**, 157-171.

Lv, H.Y, Tang, Y.S., Zhang, L.F., Cheng, Z.B. and Zhang, Y.N. (2019), "Analysis for mechanical characteristics and failure models of coal specimens with non-penetrating single crack", *Geomech. Eng*., **17**(4), 355-365. https://doi.org/10.12989/gae.2019.17.4.355.

Ma, D., Li, Q., Cai, K., Zhang, J., Li, Z., Hou, W., Sun, Q., Li, M. and Du, F. (2023), "Understanding of water inrush disaster in weak geological structure of deep mining engineering: Seepage erosion model considering tortuosity", *J. Central South Univ*., **30**(2), 517-529. https://doi.org/10.1007/s11771-023-5261-4.

Ma, D., Rezania, M., Yu, H.S. and Bai, H.B. (2017), "Variations of hydraulic properties of granular sandstones during water inrush: effect of small particle migration", *Eng. Geol*., **217**, 61-70. https://doi.org/10.1016/j.enggeo.2016.12.006.

Mahmoodzadeh, A., Mohammadi, M., Abdulhamid, S.N., Ali, H.F.H., Ibrahim, H.H. and Rashidi, S. (2022), "Forecasting tunnel path geology using Gaussian process regression", *Geomech. Eng*., **28**(4), 359-374, https://doi.org/10.12989/gae.2022.28.4.359.

Mandal, A., Basantaray, A.K., Chandroth, A. and Mishra, U. (2019), "Integrated geophysical investigation to map shallow surface alteration/fracture zones of Atri and Tarabalo hot springs", *Geothermics*, **77**, 24-33. https://doi.org/10.1016/j.geothermics.2018.08.007.

Maruvanchery, V. and Kim, E. (2017), "Effects of water on rock fracture properties: Studies of mode I fracture toughness, crack

propagation velocity, and consumed energy in calcite-cemented sandstone", *Geomech. Eng*., **17**(1), 57-67. https://doi.org/10.12989/gae.2019.17.1.057.

Munoz, H., Taheri, A. and Chanda, E.K. (2016), "Pre-peak and post-peak rock strain characteristics during uniaxial compression by 3D digital image correlation", *Rock Mech. Eng. Rock*, **49**(7), 2541-2554. https://doi.org/10.1007/s00603-016-0935-y.

Priest, S D. and Hudson, J.A. (1976), "Discontinuity spacings in rock", *Int. J. Rock Mech. Min. Sci. Geomech. Abstracts*, **13**(5), 135-148. https://doi.org/10.1016/0148-9062(76)90818-4.

Samanta, M., Punetha, P. and Sharma, M. (2018), "Effect of roughness on interface shear behavior of sand with steel and concrete surface", *Geomech. Eng*., **14**(4), 387-398. https://doi.org/10.12989/gae.2018.14.4.387.

Shao, J.L. (2022), Research on Seepage Catastrophic Characteristics and Water Inrush Mechanism of Hidden Fractures in Coal Seam Floor under Mining Effect.Shandong University of Science and Technology.

Shi, L. (2009), "Summary of research on mechanism of water-inrush from seam floor", *J. Shandong Univ. Sci. Technol. Nat. Sci*., **3**, 17-23. (in Chinese)

Sun, K.M. and Xin, L.W. (2016), "Seepage law of rough fracture during loading-unloading process considering 3D topograply characteristics", *Rock Soil Mech*., **37**(2), 161-166.

Sweetenham M.G., Maxwell, R.M. and Santi, P.M. (2017), "Assessing the timing and magnitude of precipitation-induced seepage into tunnels bored through fractured rock", *Tunn. Undergr. Sp. Tech*., **65**, 62-75. https://doi.org/10.1016/j.tust.2017.02.003.

Tatone, B.S.A. and Grasselli, G. (2015), "A calibration procedure for twodimensional laboratory-scale hybrid finite-discrete element simulations", *Int. J. Rock Mech. Min. Sci*., **75**, 56-72. https://doi.org/10.1016/j.ijrmm s.2015.01.011.

Vaziri, M.R., Tavakoli, H. and Bahaaddini, M. (2022), "2D numerical study of the mechanical behaviour of non-persistent jointed rock masses under uniaxial and biaxial compression tests", *Geomech. Eng*., **28**(2), 117-133. https://doi.org/10.12989/gae.2022.28.2.117.

Wang, J., Yang, Y. and Kong, D. (2016), "Failure mechanism and control technology of Longwall coal face in large-cutting-height mining method", *Int. J. Min. Sci. Technol*., **26**(1), 111-118. https://doi.org/CNKI:SUN:ZHKD.0.2016-01-017.

Wang, Q., Gao, H., Yu, H., Jiang, B. and Liu, B. (2019), "Method for measuring rock mass characteristics and evaluating the grouting-rReinforced effect based on digital drilling", *Rock Mech. Eng. Rock*, **52**(3), 841-851. https://doi.org/10.1007/s00603-018-1624-9.

Wang, Z., Wei, L., Bi, L., Qiao, L., Liu, R. and Jie, L. (2018), "Estimation of the REV size and equivalent permeability coefficient of fractured rock masses with an emphasis on comparing the radial and unidirectional flow configurations.rock mechanics", *Eng. Rock*, **6**, 1-15. https://doi.org/10.1007/s00603-018-1422-4.

Wu, C., Chu, J., Wu, S. and Hong, Y. (2019), "3D characterization of microbially induced carbonate precipitation in rock fracture and the resulted permeability reduction", *Eng. Geol*., **24**(9), 23-30.

Wu, J. (2014), "Progress problems and prospects of prevention and control technology of mine water and reutilization in China", *J. China Coal Soc*., **39**(5), 795-805. https://doi.org/10.13225/j.cnki.jccs.2014.0478.

Wu, J., Cui, F.P., Zhao, S.Q., Liu, S.J., Ceng, Y.F. and Gu, Y.W. (2013), "Type classification and main characteristics of mine water disasters", *J. China Coal Soc*., **38**(4), 561-565. https://doi.org/10.13225/j.cnki.jccs.2013.04.015.

Xing, H.L. and Makinouchi, A. (2000), "A node-to-point contact element strategy and its applications", RIKEN REVIEW, 35-39

Xing, H.L., Makinouchi, A. and Mora, P. (2007), "Finite element modeling of interacting fault systems", *Phys. Earth Interiors Planetary*, **163**(1-4), 106-121. https://doi.org/10.1016/j.pepi.2007.05.006.

Yang, J., Jiabin, Dong, Feng Gao , Jianguo Wang (2019), "Evaluation of water permeability of rough fractures based on a self-affine fractal model and optimized segmentation algorithm", *Adv. Water Resour*., **129**, 99-111. https://doi.org/10.1016/j. advwat res.2019.05.007.

Yang, T., Tang, C., Tan, Z., Zhu, W. and Feng, Q. (2007), "State of the art of inrush models in rock mass failure and developing trend for prediction and forecast of ground water inrush", *Chinese J. Rock Mech. Eng*., **26**(2), 268-277.

Yang, T.H., Shi, W.H., Liu, H.L., Yang, B., Xin, Y. and Liu, Z.B. (2017), "A non - linear flow model based on flow translation and its application in the mechanism analysis of water inrush through collapse pillar", *J. China Coal Soc*., **42**(2), 315-321. https://doi.org/10.13225/j.cnki.jccs.2016.6008.

Yao, B., Wang, L., Wei, J., Li, Z. and Liu, X. (2018), "A deformation-seepage-erosion coupling model for water outburst of Karst collapse pillar and its application", *J. China Coal Soc*., **43**(7), 2007-2013. https://doi.org/10.13225/j.cnki.jccs.2017.1276.

Yin, L. (2011), "Basic experimental study on water-inrush mechanism of floor in deep mining", *Shandong Univ. Sci. Technol*., https://doi.org/10.7666/d.D301269.

Yin, L., Guo, W. and Lu, C. (2017), "Patterns of the water-inrush hazard in the floor strata in deep mines and its catastrophic characteristics", *J. Min. Saf. Eng*., **34**(3), 459-463. https://doi.org/10.13545/j.cnki.jmse.2017.03.09.

Yosseff, H.H. (2003), "Keyblock stability in seismically active rock slopes—Snake Path Cliff", Masada. *J. Geotech. Geoenviron. Eng*., **129**(8), 697-705. https://doi.org/10.1061/(ASCE)1090-0241(2003)129:8(697)

Yuan, F., Ma, K., Zhuang, D., Wang, Z. and Sun, X. (2019), "Preparation mechanism of water inrush channels in bottom floor of Dongjiahe Coal Mine based on microseismic monitoring", *J. China Coal Soc*., **44**(6), 1846-1856. https://doi.org/10. 13225 / j. cnki. jccs. 2018. 0941.

Zhang, B., Bai, H. and Zhang, K. (2016), "Research on permeability characteristics of karst collapse column fillings in complete stress-strain process", *J. Min. Saf. Eng*., **33**(4), 734-740. https://doi.org/10.13545/j.cnki.jmse.2016.04.025.

Zhang, J., Zhang, Y. and Liu, T. (1997), "Rock mass seepage and the coal floor water bursting", Beijing: Geological Publishing House

Zhang, W., Yuan, J., Wang, Z., *et al*. (2017), "An experimental study on compressive shear seepage laws of mining-induced fractured rock mass", *Rock Soil Mech*., **38**(9), 2473-2479.

Zhang, Y. (2009), "Numerical simulation on forecasting water in flow and characteristic of over burden failure based on fluid-solid coupling theory", *J. China Coal Soc*., **34**(5), 610-613.

Zhang, Y., Zhang, C. and Zhao, F. (2015), "Dynamic evolution rules of mining-induced fractures in different floor area of short-distance coal seams", *J. China Coal Soc.*, **40**(4), 786-792. https://doi.org/10.13225/j.cnki.jccs.2014.3011.

Zhao J., Zhou, H., Xue, D., Su, T., Deng, H. and Yang, H. (2019), "Expansion law of seepage path in the concealed structural floor of coal seam in deep confined water", *J. China Coal Soc*., **44**(6), 1836-1845. https://doi.org/10. 13225/j. cnki. jccs. 2018. 0844.

Zhao, J., Jiang, N., Yin, L. and Bai, L. (2019), "The effects of mining subsidence and drainage improvements on a waterlogged area", *Bull. Eng. Geol. Environ*., **78**(5). https://doi.org/10.1007/s10064-018-1356-9.

Zhao, J., Juntao, C., Huilin, X., Zhao, Z. and Xinguo, Z. (2021), "Dynamic mechanical response and movement evolution

characteristics of fault systems in the coal mining process", *Pure Appl. Geophys*., **179**(1). https://doi.org/10.1007/s00024-021-02905-w.

Zhao, J., Liu, Q., Jiang, C. and Wang, D. (2022), "Application of rock mass index in the prediction of mine water inrush and grouting quantity", *Geomech. Eng*., **30**(6), 503-515. https://doi.org/10.12989/gae.2022.30.6.503.

Zhao, J., Yin, L. and Guo, W. (2018a), "Influence of three-dimensional roughness of rock fracture on seepage characteristics based on the digital image technology", *Arab J. Geosci*., **11**(778), 1-12.

Zhao, J., Yin, L. and Guo, W. (2018b), "Stress–seepage coupling of cataclastic rock masses based on digital image technologies", *Rock Mech. Rock Eng*., **51**(8), 2355-2372. https://doi.org/10.1007/s00603-018-1474-5.

Zhou, F., Sun, W.B., Shao, J.L., Kong, L.J. and Geng, X.Y. (2020), "Experimental study on nano silica modified cement base grouting reinforcement materials", *Geomech. Eng*., **20**(1), 67-73. https://doi.org/10.12989/gae.2020.20.1.067.